targets

MDPI

Article

Semisynthetic Flavonoids as GSK-3β Inhibitors: Computational Methods and Enzymatic Assay

Heberth de Paula [1,*], Fernanda Souza [2], Lara Ferreira [2], Jéssica A. B. Silva [3], Rayssa Ribeiro [3], Juliana Vilachã [4,*], Flávio S. Emery [5], Valdemar Lacerda, Jr. [6] and Pedro A. B. Morais [3]

1 Department of Pharmacy, Federal University of Espírito Santo, Alegre 29500-000, Espirito Santo, Brazil
2 Postgraduate Program in Chemical Science and Technology, Federal University of ABC, Santo André 09280-560, São Paulo, Brazil; fer.chmst@gmail.com (F.S.); larachavesufes@gmail.com (L.F.)
3 Graduate Program in Agrochemical, Department of Chemistry and Physics, Federal University of Espírito Santo, Alegre 29500-000, Espírito Santo, Brazil; rayssaribeiro048@gmail.com (R.R.); pedro.morais@ufes.br (P.A.B.M.)
4 Department of Chemistry, School of Life Sciences, University of Warwick, Gibbet Hill Campus, Coventry CV4 7AL, UK
5 Department of Pharmaceutical Sciences, Faculty of Pharmaceutical Sciences of Ribeirão Preto, University of São Paulo, Ribeirão Preto 14040-903, São Paulo, Brazil; flavioemery@fcfrp.usp.br
6 Graduate Program in Chemistry, Department of Chemistry, Federal University of Espirito Santo, Vitória 29075-910, Espírito Santo, Brazil; valdemar.lacerda@ufes.br
* Correspondence: heberth.paula@ufes.br (H.d.P.); juliana.vilacha@warwick.ac.uk (J.V.)

Abstract: Glycogen synthase kinase-3 beta (GSK-3β) plays a crucial role in multiple cellular processes and is implicated in different types of cancers and neurological disorders, including Alzheimer's disease. Despite extensive efforts to develop novel GSK-3β inhibitors, the discovery of potent and selective lead compounds remains a challenge. In this study, we evaluated the GSK-3β inhibitory potential of semisynthetic flavonoid derivatives, which exhibited sub-micromolar activity. To gain further insights, we employed molecular docking, molecular dynamics simulations, and pharmacokinetic profile predictions. The docking studies revealed that the most potent inhibitor, compound 10, establishes key interactions with the ATP-binding site. Molecular dynamics simulations further confirmed that compound 10 maintains stable interactions with GSK-3β throughout the simulation. Additionally, pharmacokinetic predictions identified compound 3 as a promising candidate for Alzheimer's disease therapy due to its ability to cross the blood–brain barrier. These findings suggest that, within the studied flavonoid derivatives, these compounds (particularly 10 and 3) hold potential as lead compounds for GSK-3β inhibition. The combination of strong enzymatic inhibition, stable binding interactions, and favorable pharmacokinetic properties highlights their promise for further development in cancer and neurodegenerative disease research.

Keywords: semisynthesis; triazole; GSK-3β inhibitory activity; Alzheimer's disease; cancer

check for updates

Academic Editor: Huangxian Ju

Received: 28 February 2025
Revised: 27 March 2025
Accepted: 10 April 2025
Published: 15 April 2025

Citation: de Paula, H.; Souza, F.; Ferreira, L.; Silva, J.A.B.; Ribeiro, R.; Vilachã, J.; Emery, F.S.; Lacerda, V., Jr.; Morais, P.A.B. Semisynthetic Flavonoids as GSK-3β Inhibitors: Computational Methods and Enzymatic Assay. *Targets* **2025**, *3*, 13. https://doi.org/10.3390/targets3020013

Copyright: © 2025 by the authors. Licensee MDPI, Basel, Switzerland. This article is an open access article distributed under the terms and conditions of the Creative Commons Attribution (CC BY) license (https://creativecommons.org/licenses/by/4.0/).

1. Introduction

The glycogen synthase kinase-3 (GSK3) gene family includes *GSK3A* and *GSK3B*, which are closely related. *GSK3A* encodes a 51 kDa protein, while *GSK3B* encodes a slightly smaller protein of 47kDa [1]. These two isoforms share approximately 85% sequence similarity overall, with their catalytic domains being fully conserved (100%). Structurally, GSK-3α and GSK-3β are distinguished by unique N- and C-terminal regions. Both proteins adopt a bilobed conformation, where the larger, globular C-terminal domain contains the catalytic site, and the smaller N-terminal domain houses the ATP-binding region. As a

kinase, the ATP-binding site is positioned within a cleft between these two domains [2]. Glycogen synthase kinase-3 beta is a ubiquitously expressed serine/threonine kinase and initially revealed as a pivotal enzyme for glycogen metabolism [3]. This protein is now recognized as a regulator of diverse cellular functions [4] related to oncogenesis and neurological diseases and its dysfunction can result in diabetes, cancer, and psychiatric conditions, such as schizophrenia, bipolar disorder, depression, and Alzheimer's Disease (AD) [5]. Control of the activity of diverse metabolic, signaling, and structural proteins by GSK-3 occurs through the phosphorylation of several substrates catalyzed by this protein [6].

Tumor suppression related to GSK-3β consists of its ability to phosphorylate pro-oncogenic pathways such as c-Jun [7], c-Myc [8], cyclin D1 [9], and β-catenin [10] for ubiquitin-dependent proteasomal degradation. Moreover, recently it was described in the literature that GSK-3β is a positive regulator of cancer cell proliferation and survival, showing further support for GSK-3β as a therapeutic target [3]. GSK-3β up-regulates the function of nuclear factor (NF)-kB, interfering in pathways associated with cell proliferation, the synthesis of pro-tumorigenic cytokines, and the progression of resistance to apoptosis [11].

At the time of the preparation of this report, 50 million individuals are affected by dementia worldwide [12]. As a consequence of growing life expectancies, the number of patients diagnosed with this neurological disorder is estimated to triple by 2050. Alzheimer's disease is a type of dementia usually observed in the elderly with a growing number of incident cases per year [13]. The morphology of AD reveals that damage to central nervous system (CNS) is initiated 10 to 20 years before any clinical problems are diagnosed [14]. GSK-3 has an intrinsic relationship with AD since it participates in the hyperphosphorylation of tau protein, a crucial structure in neurofibrillary tangles that is known to be one of the hallmarks of AD. Further investigation revealed that GSK-3 is involved in the control of several neuronal processes which are abnormal during AD pathogenesis, such as the production of amyloid-β (Aβ) peptide or Aβ-induced cell death, axonal transport, cholinergic function, and adult neurogenesis or synaptic functioning [15].

Molecular dynamics (MD) simulations, a hallmark computational technique used to study (bio)(macro)molecules, have been widely used to explore unbiased conformations of ligands and receptors, accounting for their dynamic flexibility and interactions over time [16,17] in order to overcome the 'lock-and-key' theory in which a static receptor is adopted to dock a small molecular entity without any conformational modification. The relevance of this improved technique is corroborated by crystallographic studies which have convincingly revealed the need to explore protein flexibility in ligand binding. MD applies simple approximations based on Newtonian physics to promote atomic motions and optimize computational efforts [18]. In addition, numerous reports using MD and experimental data in the literature can be seen to validate this computational technique [19] and a good agreement has been observed [20].

Flavonoids have been explored through numerous in vitro and in vivo studies, which have elucidated that this class of natural products interferes with processes and pathways relevant to AD and cancer progression, such as amyloid β peptide and tau pathology, increases in brain-derived neurotrophic factor, inflammation, oxidative stress, neurogenesis and the regulation of apoptosis, the cell cycle, metabolism, and cells' longevity, respectively. So far, more than 5000 compounds showing a flavonoid skeleton, which are encountered almost ubiquitously in plants broadly used in the human diet, have been described in the literature [21]. The molecular mechanisms of action presented by flavonoids against these disorders are detailed in the literature, including the flavonoid-mediated regulation of tau phosphorylation and aggregation related to proline-directed kinases such as GSK-3 [22],

CDK5 [23], and members of the MAPK family [24], the degradation and inhibition of the aggregation of amyloid β peptide involving the estrogen receptor α (ERα)-mediated activation of the PI3K/Akt pathway, and activation of the pro-ADAM10 cleavage enzyme furin through a PI3K-independent mechanism [25] and the Akt/GSK-3 signaling pathway, which is dysregulated in several tumors [21].

The strategy of creating alternative treatments for AD and cancer by targeting amyloid β peptide, tau protein, and regulatory kinases is widely used to produce novel therapeutics derived from natural products and their semisynthetic derivatives. In this context, flavonoids are particularly attractive due to their structural diversity and established activity on kinase-mediated pathways, including those involving GSK-3β. Herein, we report the enzymatic evaluation of sixteen flavonoid derivatives (Figure 1) against GSK-3β, supported by binding mode prediction through molecular docking, molecular dynamics simulations, and pharmacokinetic profiling, which corroborate the sub-micromolar IC_{50} values obtained for the most active compounds, **3**, **5**, and **10**.

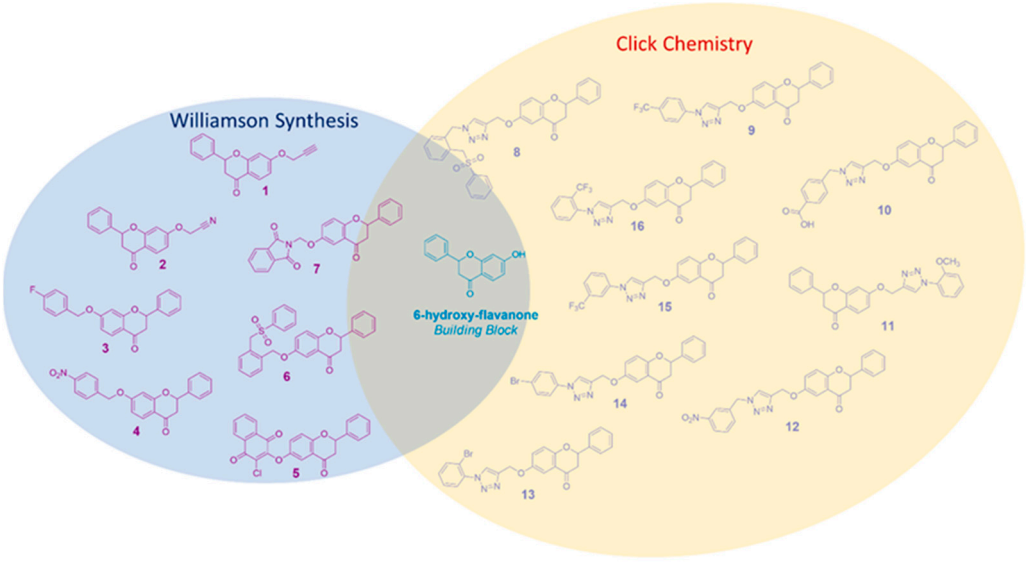


Figure 1. O-alkylated **1**–**7** and triazole **8**–**16** derivatives of 6-hydroxy-flavanone.

The 6-Hydroxyflavanone scaffold was selected as the core scaffold for modification based on our preliminary MD studies, which suggested favorable interactions with GSK-3β. Despite the increasing interest in flavonoid-based GSK-3β inhibitors, a comprehensive literature survey revealed that 6-hydroxyflavanone derivatives have not previously been investigated for their potential GSK-3β-inhibitory activity. Therefore, this study aims to explore the uncharted potential of this underexplored scaffold and to provide the first experimental data on its inhibitory profile.

2. Materials and Methods

2.1. Chemical Synthesis

The O-alkylated **1**–**7** and triazole **8**–**16** derivatives of 6-hydroxy-flavanone (Figure 1) were previously synthesized by our group [26].

2.2. Biological Testing

GSK-3β Enzymatic Assay

The GSK-3β-inhibitory activity of sixteen flavonoid derivatives was measured using the "GSK-3β kinase enzyme system" (PROMEGA). In brief, to make a final reaction enzyme concentration of 1 nM, GSK-3β human was diluted in a solution with 4Xre-

action buffer and dithiothreitol (200 M). A 2.5X ATP/substrate mixture was made by mixing 4X reaction buffer, 100 M ATP, and 1 mg·mL^{-1} GSK-3 substrate (YRRAAVPPSP-SLSRHSSPHQ(pS)EDEEE) derived from human muscle glycogen in a 1:1:2 ratio. Inhibitors were solubilized on DMSO (pure, SIGMA ALDRICH, St. Louis, MO, USA) to make 20 mM, 2 mM, and 0.2 mM solutions (with final reaction concentrations of 1 mM, 1 µM, and 1 nM, respectively, and always on 5% DMSO).

The reaction was carried out on a 384 low-volume plate. First, 1 µL of inhibitor, 2 µL of enzyme solution, and 2 µL of ATP/substrate mix were added to each well. One well included DMSO instead of an inhibitor to make a reaction standard with 100 percent enzyme activity. Instead of inhibitor and enzyme, DMSO was added to one well to make a reaction standard with 0% enzyme activity. The final volume of all wells was the same. The plate was incubated for 60 min at 30 °C. Then, 5 µL ADP-GLO® reagent was applied to each well to deplete any remaining ATP after the reaction. After 40 min of incubation at 30 °C, the reaction was complete. Finally, 10 µL of Kinase Detection Reagent® was applied to each well to convert the ADP to freshly synthesized ATP and conduct the Luciferase/Luciferin reaction. After 60 min of incubation at 30 °C, the luminescence was measured (integration time 0.5–1 s). All of these processes were carried out in triplicate for each concentration/inhibitor. The findings were standardized to a 100 percent enzyme activity level using relative light units (RLUs). GraphPad Prism 7.00 software (GraphPad Software, Inc., Boston, MA, USA) was used to measure the IC_{50} using a non-linear regression log (inhibitor) vs. a response normalized.

2.3. Computational Methods

Molecular Docking

A molecular docking study was carried out using GOLD 2021.1.0 software to analyze the interactions between the most active inhibitors, **3**, **5**, and **10**, and the biological target GSK-3β. The crystallographic structure GSK-3β was obtained from the Protein Data Bank www.rcsb.org/ (accessed on 12 May 2023, PDB code 4ACG, resolution 2.60 Å). The parameters were chosen by testing several during the redocking step modifying (a) the score function, (b) the cavity diameter at the ATP-binding site around the crystallographic ligand, (c) the flexibilization of the amino acid residues, and (d) the presence of structural water molecules. Then, the lowest RMSD (Root-Mean-Square Deviation) value was obtained from the overlap between the redocking pose and the crystallographic ligand.

An RMSD value lower than 2.0 Å is considered satisfactory for the parameters to be applied in docking simulations with the most active inhibitors, **3**, **5**, and **10**. The best configuration of each inhibitor was selected and analyzed with PyMOL(TM) 3.1.1 software and Proteins Plus (http://proteins.plus, accessed on 30 July 2024). The main interactions between the best configuration of inhibitors **3**, **5**, and **10** and the protein were highlighted as described.

2.4. Molecular Dynamics

The complexes resulting from the docking of compounds **3**, **5**, **10** and SB415286 were used for all-atom MD simulations, including the enzymes in the apo form, using the GROMACS 2022.3 package and the CHARMM36 force field, last updated in July 2022 [27,28]. Each complex was solvated inside a dodecahedral box with a three-point water molecules model (TIP3P), allowing for a minimum of 1 nm of marginal distance between the protein and each side of the simulation box [29]. The net charge of the simulation system was neutralized by counter-ions Na^+ and Cl^- that replace water molecules and, to replicate the physiological conditions of the cell environment, we increased the concentration to 150 mM [30].

The simulation was conducted in three stages and a force constant of 1000 kJ·mol^{-1}·nm^{-2} was used to constrain all the heavy atoms. The first energy minimization step involved the initial optimization of each system geometry using 5000 iterations with the steepest descent algorithm. The subsequent step involved equilibrating the system in two stages, where the system was conditioned for 100,000 iterations (100 ps) in each stage (with a timestep of 2 fs). We performed the first stage of equilibration under a constant set of particle numbers, volumes, and temperatures (NVTs). Then, we performed the second stage of equilibrium under a constant set of particle numbers, pressures, and temperatures (NPTs) at 1 atm using C-rescale barostat and 300 K using the V-rescale thermostat [31,32]. We used the Particle Mesh Ewald (PME) algorithm to calculate the electrostatic interactions, and the hydrogen bonds were constrained by the LINCS algorithm [33].

Finally, we performed the production step for 200 ns, in independent triplicates. We calculated comparative data, including the Root Mean Square Deviation and Fluctuation (RMSD and RMSF, respectively), by analyzing the MD trajectories using GROMACS 2022.3 tools. Ultimately, we estimated the binding free energy between ligands and proteins using the GROMACS module "gmx_MMPBSA" [34,35]. Additionally, an interaction map was generated using in-house Python scripts, employing the pandas, matplotlib, and seaborn libraries, along with the Protein-Ligand Interaction Profiler (PLIP) 2.4.0 [36]. PLIP was used to extract molecular interaction data from the simulations. These data were then compiled into a single data frame using pandas and visualized through scatter plots where different types of interactions were distinctly colored using matplotlib and seaborn.

2.5. Pharmacokinetic Prediction

Since ADME properties are crucial to confirm whether the semisynthetic flavonoids **3**, **5**, and **10** are potential drug candidates to serve as anticancer agents or for AD therapy, in silico calculations of molecular properties and drug-like parameters were performed based on theoretical approaches to identify drug-like requirements in the most active compounds. Molecular properties (molecular weight, LogP value, number of hydrogen bond acceptors (HBA), number of hydrogen bond donors (HBD), total polar surface area incorporated with Lipinski's rule of five were applied using the SwissADME server (http://www.swissadme.ch/index.php, accessed on 12 March 2024) [37]. We submitted the SMILES data for the selected molecules for the prediction of their physicochemical properties and for the generation of a BOILED-Egg plot, which provides data on gastrointestinal absorption and blood–brain barrier permeation [38].

3. Results

3.1. GSK-3β Inhibitory Activity of Flavonoid Derivatives

The flavonoid derivatives were evaluated for GSK-3β enzymatic inhibition using the Kinase Enzyme System (PROMEGA), which reveals the amount of ADP produced through the kinase reaction. The IC_{50} values obtained for the semisynthetic flavonoids **1**–**16** are highlighted in Table 1. Six of them showed clear sub-micromolar inhibitory activity against the triazole derivatives. Compounds **3**, **5**, **10**, **11**, and **15** exhibited a higher potency against GSK-3β with IC_{50} values ranging from 0.376 to 0.655 μM. Interestingly, the molecular hybridization strategy applied to obtain these compounds was capable of gathering well-established pharmacophoric portions, such as the triazole ring in **10** with an IC_{50} value of 0.376 μM, and the naphthoquinone nucleus in **5** with an IC_{50} value of 0.428 μM, with the flavonoid scaffold.

Table 1. Inhibitory activity of flavonoid derivatives against GSK-3β.

IC_{50} (μM)	Compound
29.08% [a]	**1**
1.211	**2**
0.467	**3**
5.941	**4**
0.428	**5**
61.89	**6**
1.589	**7**
7.476	**8**
1.426	**9**
0.376	**10**
0.655	**11**
2.027	**12**
4.52% [a]	**13**
0.959	**14**
0.607	**15**
2.752	**16**
0.096	SB415286

[a] % enzymatic activity at 1 mM.

Based on the inhibitory activity results, a preliminary SAR analysis indicates that specific structural features significantly influence GSK-3β inhibition. Notably, compounds bearing 1,2,3-triazole moieties (e.g., **10**, **11**, and **15**) demonstrated improved potency, suggesting that this heterocycle contributes favorably to interactions within the ATP-binding site, likely through hydrogen bonding and π-stacking interactions. Additionally, the naphthoquinone-substituted flavonoid (compound **5**) also showed a high inhibitory activity, which may be attributed to enhanced π-system interactions and increased molecular rigidity. In contrast, simpler O-alkylated derivatives (e.g., **1**, **2**, and **4**) exhibited weaker activity, implying that minimal substitution in the flavanone core is insufficient to establish effective binding. These findings underscore the relevance of molecular hybridization strategies that combine the flavonoid scaffold with additional pharmacophores to optimize the binding affinity and biological activity against GSK-3β.

3.2. Docking Studies

The parameters obtained from the redocking analyses performed for the docking simulations are related to the lowest RMSD values in comparison with score functions and the center of the grid box around the crystallographic ligand as highlighted in Supplementary Table S1. Water molecules were not considered as well as flexibilization of crucial amino acid residues. Then, the following parameters were applied in the docking simulations: (i) a docking box within 5 Å around the crystallographic ligand, and (ii) the Goldscore function to rank the resultant conformations. The best configurations for redocking as illustrated in Figure 2 revealed pivotal interactions with amino acids residues in the ATP-binding site in GSK-3β.

In Figure 3 is presented the best configurations for binding mode predictions for the most active compounds **3**, **5** and **10**, which stabilized the ATP-binding site of GSK-3β through interactions comprehending pivotal amino acid residues for catalytic function such as represented in Supplementary Table S2. Compounds **3**, **5** and **10** exhibited a hydrogen bond interaction with the Lys85 residue, additionally, compounds **10** and **5** showed a hydrogen bond with Cys199. Moreover, **10** and **3** performed π-stacking interactions with Phe67 (Figure 3). These interactions are capable of stabilizing the active site in proteins and corroborating the notorious enzymatic inhibitory properties of flavonoid derivatives.

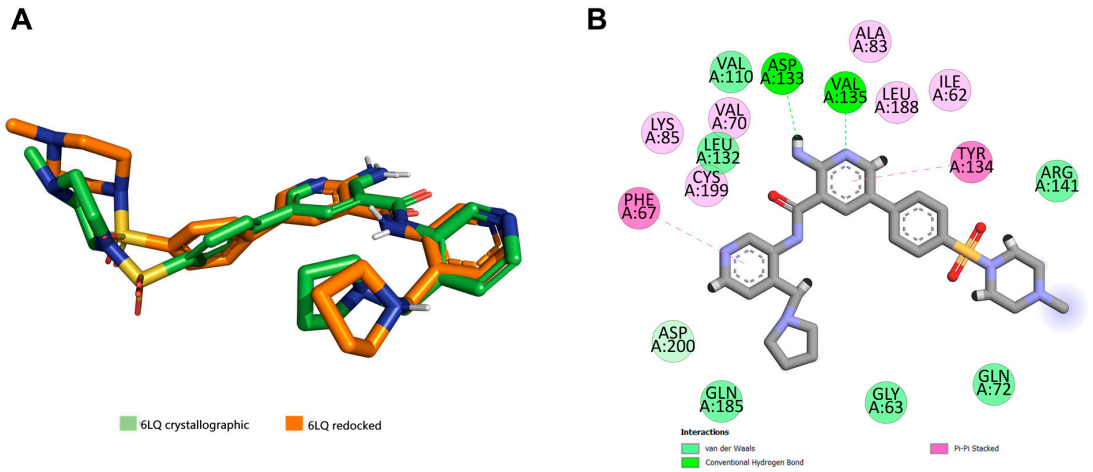


Figure 2. (**A**) Redocking result for serine/threonine kinase GSK-3β. Ligand configuration obtained from redocking in orange and 2-Amino-5-{(4-Methylpiperazin-1-yl)sulfonyl}-N-[4-(Pyrrolidin-1-ylmethyl)Pyridin-3-yl]Pyridine-3-Carboxamide in green (PDB code: 6LQ). (**B**) Two-dimensional interactions between ligand and protein. The spheres containing the residues are colored accordingly with the interaction with the ligand, with van der Waals interactions in light green, hydrogen bonds in green and pi-pi stacking in pink.

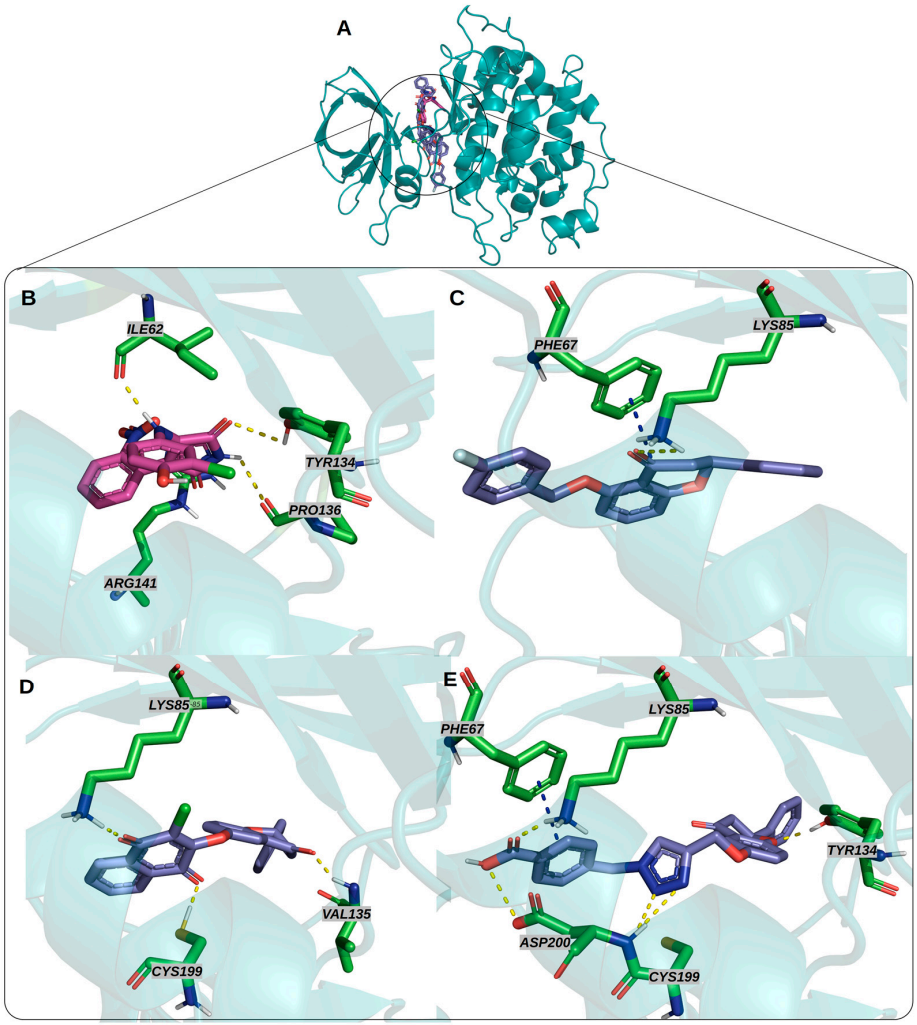


Figure 3. (**A**) Docking configurations in active site of GSK-3β with carbon atoms in pink. Binding mode prediction of (**B**) SB415286 and flavonoid derivates (**C**) **3**, (**D**) **5**, and (**E**) **10** with carbon atoms in blue. In all figures, the carbon atoms of the receptor side chain is shown in green.

3.3. Molecular Dynamics Results

To validate the molecular dynamics simulations, RMSD and RMSF analyses were performed, confirming the overall stability of the system and consistent conformational behavior across all ligand–enzyme complexes. Compound 10 showed slightly less fluctuation in key regions, suggesting stable binding interactions. Detailed results and corresponding plots are available in Supplementary Figure S1.

In addition to these analyses, the interaction map obtained further contributes to the interpretation of the stability generated in each complex. In the simulation of GSK-3 with compound **3** (Figure 4A), it can be observed that the ligand interacts predominantly with Phe67, Lys85, and Lys86 throughout the simulation, which are interactions observed in docking. These interactions are mainly of the hydrogen bond, halogen, and pi-stacking type.

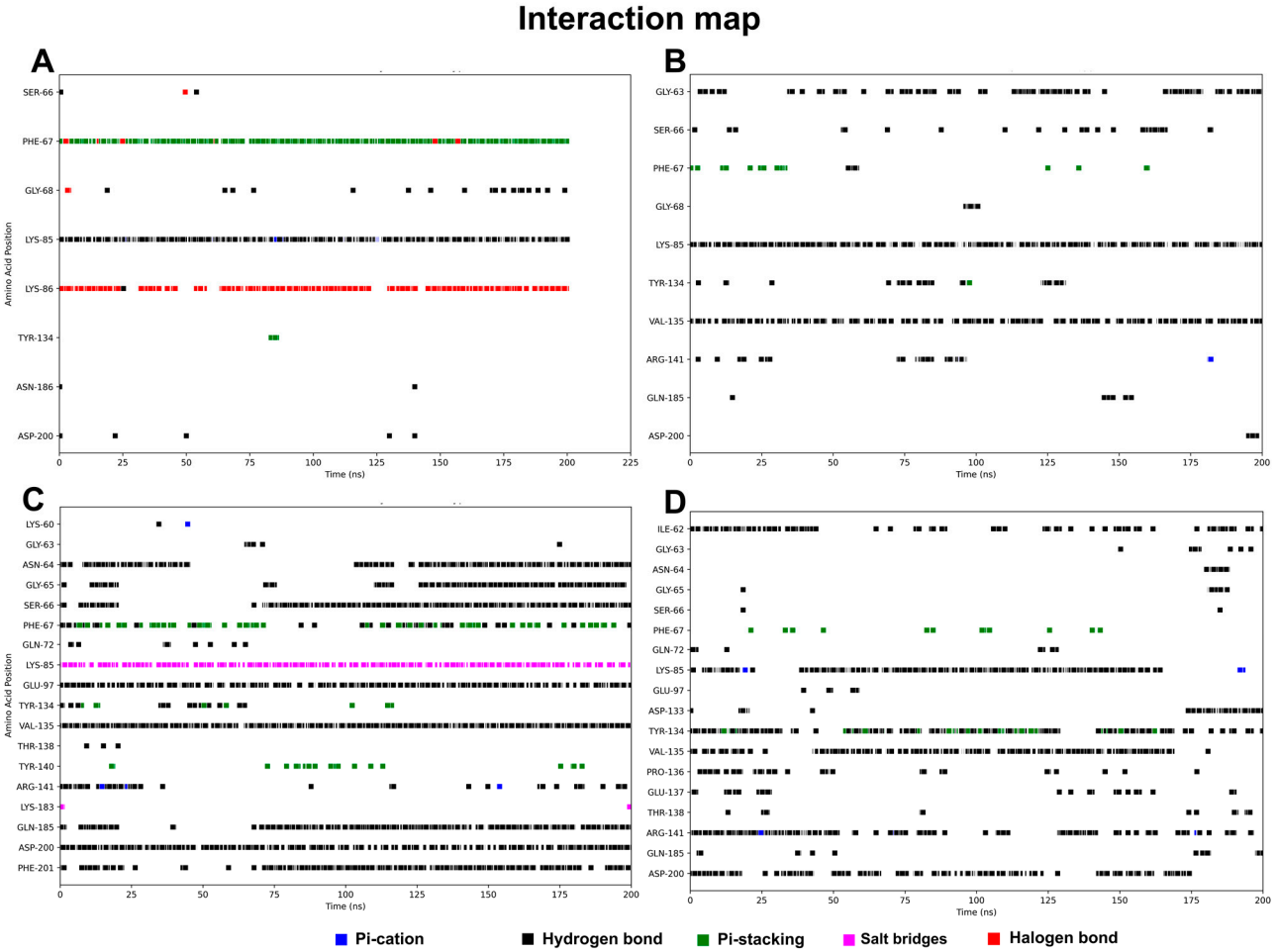


Figure 4. Interaction maps for GSK-3β in complex with compounds (**A**) **3**, (**B**) **5**, (**C**) **10**, and (**D**) SB415286.

The simulation with compound **5**-receptor complex generated a map with interactions between similar residues demonstrating differential behavior, in addition to other residues that interacted with less predominance throughout the simulation (Figure 4B). The residues in this map confirm the interactions seen in docking. The residues with the interactions with the longest residence time were Lys85, Val135, and Gly63.

The interaction pattern of the catalytic residues in SB415286 can be seen in the interaction map in Figure 4C, which was created for comparison with simulations of the derivatives. A clear similarity between the residues is noted in the simulations in which the residues with the longest residence times and interactions were Ile62, Lys85, Tyr134, Val135

Arg141, and Asp200. These interactions were principally of the hydrogen bond type, and we highlight the proximity of the residue Phe67 to those performing pi-stacking interactions. As seen in this interaction pattern, the simulation complexed with **10** surpassed the stability of the predicted interactions in addition to maintaining additional interactions with important residues. The predominant interactions are still of the hydrogen bond type, and we highlight greater stability with the residues Asn64, Gly65, Ser66, Phe67, and Lys85. Glu97, Val135, Gly185, Asp200, and Phe201 were also observed in other studies. Thus, we were able to compare the conformational stability that each ligand provides in the GSK3-β structure and justify the activities observed in the assays.

3.4. Free Energy Calculations

The MM/PBSA method was applied to calculate the binding free energy between the complexes. After obtaining the trajectories through molecular dynamics simulations, it was possible to evaluate the most stable trajectories and, thus, estimate the binding energy values between the ATP binding site of GSK-3β and compounds **3**, **5**, **10**, and SB415286 (Table 2). The binding free energy values (ΔG) for all complexes revealed estimated ΔG values less than zero, indicating a binding affinity with GSK-3β.

Table 2. Binding free energy (ΔG) values obtained for complex between GSK-3β and **3**, **5**, **10**, and SB415286.

SEM *	$\Delta G_{MM/PBSA}$	Complex
±0.12	−31.08	GSK3β-**3**
±0.44	−28.43	GSK3β-**5**
±0.83	−50.10	GSK3β-**10**
±0.69	−19.88	GSK3β-SB415286

* Standard error mean.

Compound **10** stands out with the lowest estimated value (−50.10 kcal/mol). We believe that this estimate is equivalent to the nature, quantity, and residence time of the interactions throughout the simulations. Thus, we observe that these results corroborate what was observed in the assay and docking results. Furthermore, the predominance of hydrogen bonding and pi-stacking interactions stands out, and in Figure 5, the residues that contributed most to stability, and consequently the estimated free energy value, are shown.

However, it is important to highlight that, although the binding free energy of GSK3β-10 is indeed lower (indicating a stronger interaction than GSK3β-SB415286), this does not necessarily mean that compound **10** has a more efficient inhibitory activity than SB415286, as enzymatic activity is influenced by additional factors. The lower ΔG value for the GSK3β-10 complex can be attributed to a greater enthalpic contribution, suggesting that compound **10** binds to GSK3β more stably, likely through strong interactions such as hydrogen bonds and π-stacking. These enthalpic interactions may be stronger in the case of compound **10**, with a higher density of interactions at critical points in the enzyme's active site, such as Lys85, Cys199, and Phe67, which stabilize the interaction. The formation of additional interactions in the GSK3β-10 complex could result in a more unfavorable entropic effect, as the formation of more organized complexes, with more bonds and specific interactions, may reduce the freedom of movement of the involved molecules. Teague, in his work, revealed the importance of flexibility in drug-related receptors [39]. This could partly explain the greater binding affinity of compound **10**, but not necessarily its greater inhibitory activity. Entropy may be favorable in the case of SB415286, where a smaller number of more specific and flexible interactions could result in a greater conformational freedom of the complex, allowing the enzyme to function more efficiently in the context of enzymatic activity.

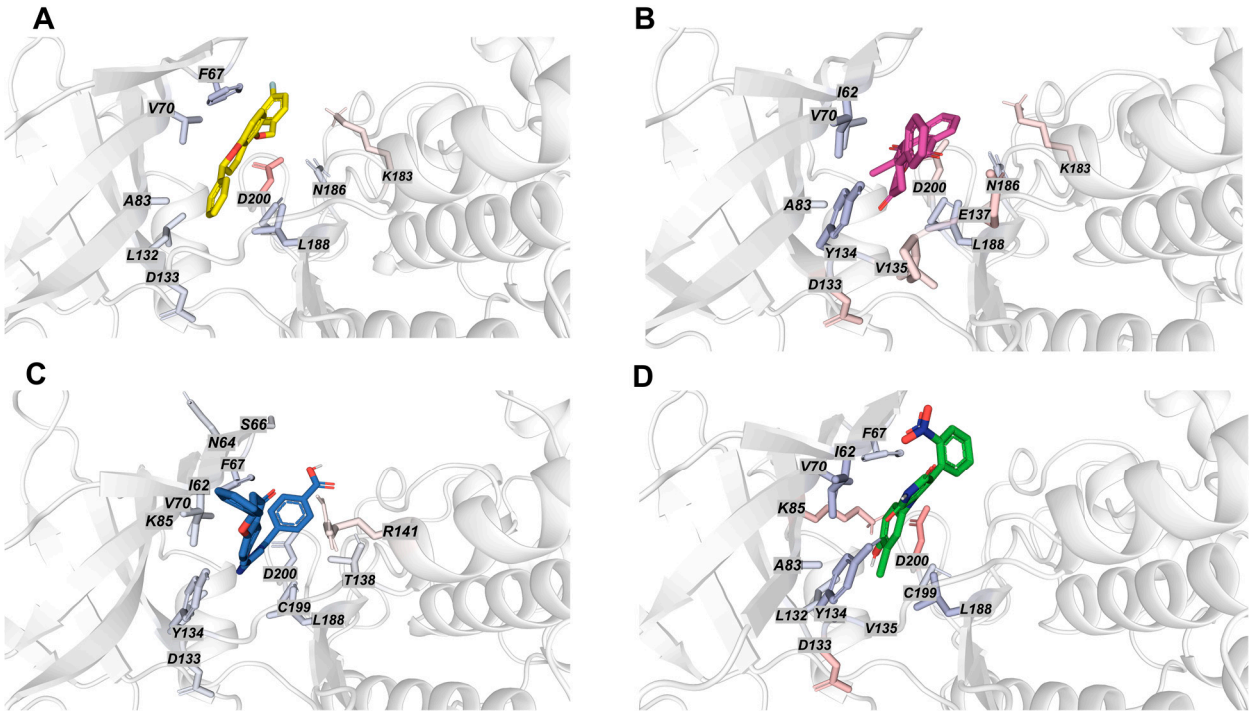


Figure 5. MM/PBSA decomposition analysis per residue to evaluate the energy contribution of the residue of GSK-3β with compounds (**A**) **3**, (**B**) **5**, (**C**) **10**, and (**D**) SB415286. Carbon atoms of different compounds are colored yellow, pink, blue and green, respectively. The side chain atoms of the protein, when presentend as sticks are colored accordingly to their contribution to binding.

3.5. Pharmacokinetic Prediction of Selected Compounds

As is well established, absorption, distribution, metabolism, and excretion (ADME) are essential properties necessary to ensure a drug's efficacy and are intrinsically related to its physicochemical profile [37].

Thus, initially, through the TPSA and WLOGP parameters and physicochemical data, the BOILED-Egg statistical plot was obtained to predict the penetration of the blood–brain barrier (BBB) and gastrointestinal absorption of compounds **3**, **5**, and **10** (Figure 6A). These parameters are represented in an ellipse shape. Compounds present in the yellow ellipse are related to a greater probability of penetration into the BBB. On the other hand, compounds in the white region are predicted to display extended gastrointestinal absorption. In addition, compounds in the gray region are identified as non-bioavailable for oral administration.

Thus, compound **3** was predicted to passively permeate the blood–brain barrier and, consequently, was considered as the most promising drug candidate for AD therapy. It is worth noting that a remarkable challenge facing a GSK-3β inhibitor in the drug development process is its specific brain distribution, since is necessary to cross the blood–brain barrier and to regulate the levels of GSK-3β in the brain [40].

Furthermore, a bioavailability radar, which enables a first glance at the drug-properties of a new molecular entity, was generated in relation to six pharmacokinetic parameters, lipophilicity (XlogP3 between −0.7 and 5.00), molecular weight (ranging 150 to 500 g/mol), polarity (TPSA between 20 and 130 $Å^2$), insolubility (log S between 0 and 6), unsaturation (sp3 portion ranging 0.25 and 1), and flexibility (number of flexible bonds between 0 and 9). Oral bioavailability is illustrated in the colored region. It is worth noting that compound **10**, the most active GSK-3β inhibitor, revealed a clear pharmacokinetic profile on the radar in relation to the commercial inhibitor SB415286 (Figure 6B).

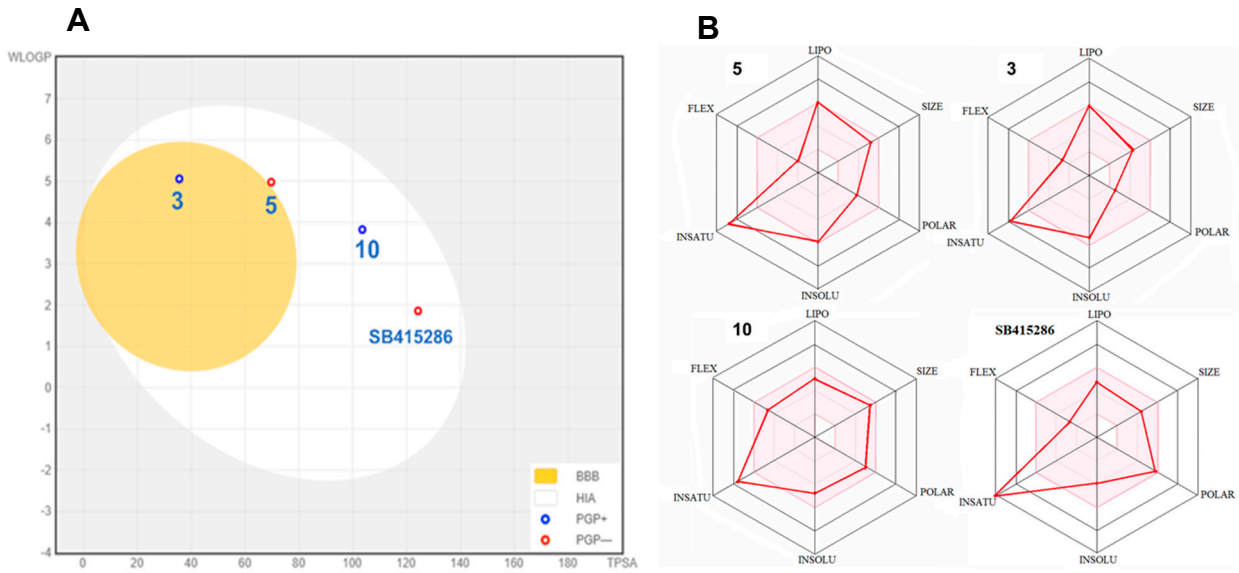


Figure 6. (**A**) BOILED-Egg graph for GSK-3β inhibitors **3**, **5**, **10**, and SB415286. (**B**) Bioavailability Radar for the most active GSK-3β inhibitors **3**, **5**, and **10**, and commercial inhibitor SB415286. The colored region is the specific physicochemical space for predicted oral bioavailability calculated by SwissADME with the darker red line representing the compound performance in the specific physicochemical characteristic.

Finally, Lipinski's rule of five states that, based on orally active drugs, a small molecule is considered to be a drug candidate if it has a molecular weight of less than 500 g·mol^{-1}, a lipophilicity, expressed as cLogP, less than 5, less than ten hydrogen acceptor groups, and less than five hydrogen donor groups [41]. The three inhibitors studied, **3**, **5**, and **10**, do not violate Lipinski's rule of five, corroborating the interesting pharmacokinetic profile of these flavonoid derivatives.

4. Discussion

The results of this study reinforce the relevance of semisynthetic flavonoids as promising inhibitors of GSK-3β, with potential applications in neurodegenerative diseases and cancer [21,42,43]. The enzymatic activity observed for compounds **3**, **5**, and **10**, with submicromolar IC_{50} values, suggests efficient interactions with the enzyme's catalytic site. Computational studies corroborate these findings, indicating crucial molecular interactions that may justify the observed inhibitory activity.

Molecular docking analysis revealed that the most active compounds exhibited recurring interactions with key residues essential for the catalytic function of GSK-3β. The Lys85 residue, identified in all complexes, stabilizes ATP in the active site, and its interaction with the inhibitors may prevent substrate phosphorylation, a mechanism frequently associated with GSK-3β inhibition [44]. Additionally, Cys199, observed in the interactions of compounds **5** and **10**, has been reported in the literature as a crucial site for allosteric modulation of the protein, potentially contributing to the efficacy of these compounds. The Phe67 residue, involved in π-stacking interactions with compounds **3** and **10**, plays a key role in stabilizing the molecule within the active site, enhancing binding affinity.

Molecular dynamics simulations provided additional evidence for the stability of the complexes and the impact of inhibitors on GSK-3β flexibility. The RMSD analysis demonstrated that compounds **3**, **5**, and **10** maintained stable interactions over 200 ns of simulation, indicating that the ligands do not induce significant conformational perturbations in the protein [45,46]. RMSF calculations revealed that the largest structural displacements occurred in loop regions near the active site, suggesting a possible impact

on the enzyme's catalytic dynamics. Notably, compound **10** exhibited the most stable and long-lasting interaction profile, which may be related to the higher inhibitory potency observed for it in enzymatic assays.

The binding free energy estimates (MM/PBSA) support the experimental findings, with negative ΔG values for all complexes analyzed. Compound **10** presented the lowest binding energy compared to compounds **3** and **5**, which follow the differences observed in the interactions. This result supports the hypothesis that the presence of the triazole moiety in the compound contributes to additional interactions in the active site, increasing the stability of the protein–inhibitor complex [47].

Beyond structural analysis, pharmacokinetic property predictions indicated that compound **3** has a high probability of crossing the blood–brain barrier (BBB), suggesting its potential as a candidate for Alzheimer's disease therapy. This finding is particularly relevant, as one of the main challenges in developing GSK-3β inhibitors for neurodegenerative diseases is ensuring their efficient distribution in the central nervous system. On the other hand, compound **10**, due to its higher affinity for GSK-3β and binding stability, may be a more suitable candidate for oncological applications, where selectivity and inhibitory potency are critical factors [48].

The correlation between the computational results and experimental data reinforces the reliability of the approaches used in this study. The combination of molecular modeling, molecular dynamics, and pharmacokinetic predictions allowed for a comprehensive analysis of the interaction mechanisms of these inhibitors with GSK-3β, providing a robust foundation for future structural optimizations.

5. Conclusions

In the last twenty years, GSK-3 has attracted particular attention for the development of new molecular entities as an inhibitor due to its influence in several biochemical processes. In this work we performed GSK-3β enzymatic assay to search novel inhibitors as lead candidate and supported by computational methods. A small library of sixteen 6-hydroxyflavanone derivatives were evaluated as potential inhibitors against serine/threonine kinase GSK-3β consisting of ethers and triazole derivatives. Six of them, **3**, **5**, **10**, **11**, **14**, and **15**, were revealed to have sub-micromolar inhibitory activity. The most active compounds, **3**, **5**, and **10**, were submitted to docking simulations to predict the binding mode which showed hydrogen bonds and π-stacking interactions which are crucial for inhibitory activity. Pharmacokinetic profile prediction interestingly showed the p-fluorobenzyl derivative **3** as a lead candidate for AD since it may be able to cross blood–brain barrier and act in the CNS. Finally, the most active compounds, **3**, **5**, and **10**, were subjected to molecular dynamics simulations and free energy calculations. Thus, the results obtained in the molecular dynamics simulations reveal that compound **10** interacts more stably with the ATP binding site of this protein, which corroborated its inhibitory potential against GSK-3β.

Supplementary Materials: The following supporting information can be downloaded at: https://www.mdpi.com/article/10.3390/targets3020013/s1, Table S1. RMSD values considering score function and cavity diameter, Table S2. Interactions of the most active compounds in binding mode prediction with amino acids in GSK-3β (PDB: 4ACG), Figure S1. Molecular Dynamics information.

Author Contributions: Conceptualization, H.d.P. and P.A.B.M.; methodology, H.d.P., F.S., J.A.B.S., L.F., R.R. and J.V.; validation, F.S. and J.V.; formal analysis, H.d.P., F.S. and J.V.; investigation, P.A.B.M.; resources, F.S.E., V.L.J. and P.A.B.M.; data curation, P.A.B.M. and F.S.; writing—original draft preparation and writing—review and editing, P.A.B.M., F.S. and J.V.; visualization, H.d.P. and P.A.B.M.; supervision, P.A.B.M.; project administration, P.A.B.M. and V.L.J.; funding acquisition, P.A.B.M. and V.L.J. All authors have read and agreed to the published version of the manuscript.

Funding: This study was supported by the Brazilian Coordination for the Improvement of Higher Education Personnel (CAPES—Finance Code 001), the National Council for Scientific and Technological Development (CNPq), and the Espírito Santo Research and Innovation Support Foundation (FAPES—Call No. 120/2017). Additional support was provided by INCTBioNat (CNPq 465637/2014-0), NCQP-UFES, and the University of Warwick.

Institutional Review Board Statement: Not applicable.

Informed Consent Statement: Not applicable.

Data Availability Statement: The datasets generated and/or analyzed during the current study are publicly available at Zenodo via the following DOI: https://doi.org/10.5281/zenodo.15200314.

Acknowledgments: The authors would like to thank the CAPES and FAPES.

Conflicts of Interest: The authors declare no conflicts of interest.

References

1. Kockeritz, L.; Doble, B.; Patel, S.; Woodgett, J.R. Glycogen synthase kinase-3-an overview of an over-achieving protein kinase. *Curr. Drug Targets* **2006**, *7*, 1377–1388. [CrossRef]
2. Duda, P.; Akula, S.M.; Abrams, S.L.; Steelman, L.S.; Martelli, A.M.; Cocco, L.; Ratti, S.; Candido, S.; Libra, M.; Montalto, G. Targeting GSK3 and associated signaling pathways involved in cancer. *Cells* **2020**, *9*, 1110. [CrossRef] [PubMed]
3. Ugolkov, A.; Gaisina, I.; Zhang, J.-S.; Billadeau, D.D.; White, K.; Kozikowski, A.; Jain, S.; Cristofanilli, M.; Giles, F.; O'Halloran, T. GSK-3 inhibition overcomes chemoresistance in human breast cancer. *Cancer Lett.* **2016**, *380*, 384–392. [CrossRef]
4. Cohen, P.; Frame, S. The renaissance of GSK3. *Nat. Rev. Mol. Cell Biol.* **2001**, *2*, 769–776. [CrossRef] [PubMed]
5. Kettunen, P.; Larsson, S.; Holmgren, S.; Olsson, S.; Minthon, L.; Zetterberg, H.; Blennow, K.; Nilsson, S.; Sjölander, A. Genetic variants of GSK3B are associated with biomarkers for Alzheimer's disease and cognitive function. *J. Alzheimer's Dis.* **2015**, *44*, 1313–1322. [CrossRef]
6. Soutar, M.P.; Kim, W.Y.; Williamson, R.; Peggie, M.; Hastie, C.J.; McLauchlan, H.; Snider, W.D.; Gordon-Weeks, P.R.; Sutherland, C. Evidence that glycogen synthase kinase-3 isoforms have distinct substrate preference in the brain. *J. Neurochem.* **2010**, *115*, 974–983. [CrossRef]
7. De Groot, R.; Auwerx, J.; Bourouis, M.; Sassone-Corsi, P. Negative regulation of Jun/AP-1: Conserved function of glycogen synthase kinase 3 and the Drosophila kinase shaggy. *Oncogene* **1993**, *8*, 841–847. [PubMed]
8. Sears, R.; Nuckolls, F.; Haura, E.; Taya, Y.; Tamai, K.; Nevins, J.R. Multiple Ras-dependent phosphorylation pathways regulate Myc protein stability. *Genes Dev.* **2000**, *14*, 2501–2514. [CrossRef]
9. Diehl, J.A.; Cheng, M.; Roussel, M.F.; Sherr, C.J. Glycogen synthase kinase-3β regulates cyclin D1 proteolysis and subcellular localization. *Genes Dev.* **1998**, *12*, 3499–3511. [CrossRef]
10. Rubinfeld, B.; Albert, I.; Porfiri, E.; Fiol, C.; Munemitsu, S.; Polakis, P. Binding of GSK3β to the APC-β-catenin complex and regulation of complex assembly. *Science* **1996**, *272*, 1023–1026. [CrossRef]
11. Edderkaoui, M.; Chheda, C.; Soufi, B.; Zayou, F.; Hu, R.W.; Ramanujan, V.K.; Pan, X.; Boros, L.G.; Tajbakhsh, J.; Madhav, A. An inhibitor of GSK3B and HDACs kills pancreatic cancer cells and slows pancreatic tumor growth and metastasis in mice. *Gastroenterology* **2018**, *155*, 1985–1998.e5. [CrossRef] [PubMed]
12. Prince, M.J.; Wimo, A.; Guerchet, M.M.; Ali, G.C.; Wu, Y.-T.; Prina, M. *World Alzheimer Report 2015—The Global Impact of Dementia: An Analysis of Prevalence, Incidence, Cost and Trends*; Alzheimer's Disease International (ADI): London, UK, 2015.
13. Hebert, L.E.; Beckett, L.A.; Scherr, P.A.; Evans, D.A. Annual incidence of Alzheimer disease in the United States projected to the years 2000 through 2050. *Alzheimer Dis. Assoc. Disord.* **2001**, *15*, 169–173. [CrossRef]
14. Buchhave, P.; Minthon, L.; Zetterberg, H.; Wallin, Å.K.; Blennow, K.; Hansson, O. Cerebrospinal fluid levels ofβ-amyloid 1-42, but not of tau, are fully changed already 5 to 10 years before the onset of Alzheimer dementia. *Arch. Gen. Psychiatry* **2012**, *69*, 98–106. [CrossRef]
15. Sayas, C.L.; Ávila, J. GSK-3 and tau: A key duet in alzheimer's disease. *Cells* **2021**, *10*, 721. [CrossRef]
16. Tsai, C.-J.; Kumar, S.; Ma, B.; Nussinov, R. Folding funnels, binding funnels, and protein function. *Protein Sci.* **1999**, *8*, 1181–1190. [CrossRef] [PubMed]
17. Ma, B.; Shatsky, M.; Wolfson, H.J.; Nussinov, R. Multiple diverse ligands binding at a single protein site: A matter of pre-existing populations. *Protein Sci.* **2002**, *11*, 184–197. [CrossRef] [PubMed]
18. McCammon, J.A.; Gelin, B.R.; Karplus, M. Dynamics of folded proteins. *Nature* **1977**, *267*, 585–590. [CrossRef]
19. van Gunsteren, W.F.; Dolenc, J.; Mark, A.E. Molecular simulation as an aid to experimentalists. *Curr. Opin. Struct. Biol.* **2008**, *18*, 149–153. [CrossRef]

20. LaConte, L.E.; Voelz, V.; Nelson, W.; Enz, M.; Thomas, D.D. Molecular dynamics simulation of site-directed spin labeling: Experimental validation in muscle fibers. *Biophys. J.* **2002**, *83*, 1854–1866. [CrossRef]
21. Hole, K.L.; Williams, R.J. Flavonoids as an Intervention for Alzheimer's disease: Progress and hurdles towards defining a mechanism of action. *Brain Plast.* **2020**, *6*, 167–192. [CrossRef]
22. Hanger, D.P.; Hughes, K.; Woodgett, J.R.; Brion, J.-P.; Anderton, B.H. Glycogen synthase kinase-3 induces Alzheimer's disease-like phosphorylation of tau: Generation of paired helical filament epitopes and neuronal localisation of the kinase. *Neurosci. Lett.* **1992**, *147*, 58–62. [CrossRef] [PubMed]
23. Baumann, K.; Mandelkow, E.-M.; Biernat, J.; Piwnica-Worms, H.; Mandelkow, E. Abnormal Alzheimer-like phosphorylation of tau-protein by cyclin-dependent kinases cdk2 and cdk5. *FEBS Lett.* **1993**, *336*, 417–424. [CrossRef]
24. Drewes, G.; Lichtenberg-Kraag, B.; Döring, F.; Mandelkow, E.; Biernat, J.; Goris, J.; Doree, M.; Mandelkow, E. Mitogen activated protein (MAP) kinase transforms tau protein into an Alzheimer-like state. *EMBO J.* **1992**, *11*, 2131–2138. [CrossRef]
25. Fernandez, J.W.; Rezai-Zadeh, K.; Obregon, D.; Tan, J. EGCG functions through estrogen receptor-mediated activation of ADAM10 in the promotion of non-amyloidogenic processing of APP. *FEBS Lett.* **2010**, *584*, 4259–4267. [CrossRef]
26. Ribeiro, R.; Eloy, M.A.; Francisco, C.S.; Javarini, C.L.; Ayusso, G.M.; Da Rocha Fonseca, V.; Romão, W.; Regasini, L.O.; Araujo, S.C.; Almeida, M.O. Flavonoid derivatives targeting BCR-ABL kinase: Semisynthesis, Molecular dynamic simulations and Enzymatic inhibition. *Curr. Top. Med. Chem.* **2021**, *21*, 1999–2017. [CrossRef] [PubMed]
27. Bauer, P.; Hess, B.; Lindahl, E. GROMACS 2022.3 Source Code. 2022. Available online: https://zenodo.org/records/7037338 (accessed on 27 February 2025).
28. Huang, J.; Rauscher, S.; Nawrocki, G.; Ran, T.; Feig, M.; De Groot, B.L.; Grubmüller, H.; MacKerell, A.D. CHARMM36m: An improved force field for folded and intrinsically disordered proteins. *Nat. Methods* **2016**, *14*, 71–73. [CrossRef]
29. Jorgensen, W.L.; Chandrasekhar, J.; Madura, J.D.; Impey, R.W.; Klein, M.L. Comparison of simple potential functions for simulating liquid water. *J. Chem. Phys.* **1983**, *79*, 926–935. [CrossRef]
30. Bahrami, H.; Salehabadi, H.; Nazari, Z.; Amanlou, M. Combined Virtual Screening, DFT Calculations and Molecular Dynamics Simulations to Discovery of Potent MMP-9 Inhibitors. *Lett. Drug Des. Discov.* **2018**, *16*, 892–903. [CrossRef]
31. Bernetti, M.; Bussi, G. Pressure control using stochastic cell rescaling. *J. Chem. Phys.* **2020**, *153*, 114107. [CrossRef]
32. Bussi, G.; Donadio, D.; Parrinello, M. Canonical sampling through velocity rescaling. *J. Chem. Phys.* **2007**, *126*, 014101. [CrossRef]
33. Hess, B.; Bekker, H.; Berendsen, H.J.C.; Fraaije, J.G.E.M. LINCS: A linear constraint solver for molecular simulations. *J. Comput. Chem.* **1997**, *18*, 1463–1472. [CrossRef]
34. Valdés-Tresanco, M.S.; Valdés-Tresanco, M.E.; Valiente, P.A.; Moreno, E. Gmx_MMPBSA: A New Tool to Perform End-State Free Energy Calculations with GROMACS. *J. Chem. Theory Comput.* **2021**, *17*, 6281–6291. [CrossRef] [PubMed]
35. Kumari, R.; Kumar, R.; Lynn, A. G-mmpbsa—A GROMACS tool for high-throughput MM-PBSA calculations. *J. Chem. Inf. Model.* **2014**, *54*, 1951–1962. [CrossRef] [PubMed]
36. Salentin, S.; Schreiber, S.; Haupt, V.J.; Adasme, M.F.; Schroeder, M. PLIP: Fully automated protein–ligand interaction profiler. *Nucleic Acids Res.* **2015**, *43*, W443–W447. [CrossRef] [PubMed]
37. Daina, A.; Michielin, O.; Zoete, V. SwissADME: A free web tool to evaluate pharmacokinetics, drug-likeness and medicinal chemistry friendliness of small molecules. *Sci. Rep.* **2017**, *7*, 42717. [CrossRef]
38. Daina, A.; Zoete, V. A BOILED-Egg To Predict Gastrointestinal Absorption and Brain Penetration of Small Molecules. *ChemMedChem* **2016**, *11*, 1117–1121. [CrossRef]
39. Teague, S.J. Implications of protein flexibility for drug discovery. *Nat. Rev. Drug Discov.* **2003**, *2*, 527–541. [CrossRef]
40. Eldar-Finkelman, H.; Martinez, A. GSK-3 inhibitors: Preclinical and clinical focus on CNS. *Front. Mol. Neurosci.* **2011**, *4*, 32. [CrossRef]
41. Lipinski, C.A.; Lombardo, F.; Dominy, B.W.; Feeney, P.J. Experimental and computational approaches to estimate solubility and permeability in drug discovery and development settings. *Adv. Drug Deliv. Rev.* **2012**, *64*, 4–17. [CrossRef]
42. Britto, K.B.; Francisco, C.S.; Ferreira, D.; Borges, B.J.P.; Conti, R.; Profeti, D.; Rodrigues, L.R.; Lacerda, V.; Morais, P.A.B.; Borges, W.S. Identifying new isatin derivatives with gsk-3β inhibition capacity through molecular docking and bioassays. *J. Braz. Chem. Soc.* **2020**, *31*, 476–487. [CrossRef]
43. Atkins, R.J.; Stylli, S.S.; Luwor, R.B.; Kaye, A.H.; Hovens, C.M. Glycogen synthase kinase-3β (GSK-3β) and its dysregulation in glioblastoma multiforme. *J. Clin. Neurosci.* **2013**, *20*, 1185–1192. [CrossRef] [PubMed]
44. Zhu, J.; Wu, Y.; Xu, L.; Jin, J. Theoretical Studies on the Selectivity Mechanisms of Glycogen Synthase Kinase 3β (GSK3β) with Pyrazine ATP-competitive Inhibitors by 3DQSAR, Molecular Docking, Molecular Dynamics Simulation and Free Energy Calculations. *Curr. Comput.-Aided Drug Des.* **2019**, *16*, 17–30. [CrossRef] [PubMed]
45. Arfeen, M.; Bhagat, S.; Patel, R.; Prasad, S.; Roy, I.; Chakraborti, A.K.; Bharatam, P.V. Design, synthesis and biological evaluation of 5-benzylidene-2-iminothiazolidin-4-ones as selective GSK-3β inhibitors. *Eur. J. Med. Chem.* **2016**, *121*, 727–736. [CrossRef] [PubMed]

46. Mou, L.; Ma, Z.; Meng, X.; Li, W.; Liang, S.; Chen, X. Exploration of the selective binding mechanism of GSK3β via molecular modeling and molecular dynamics simulation studies. *Med. Chem. Res.* **2020**, *29*, 690–698. [CrossRef]
47. de Paula, H.; Bolsoni, C.S.; de Souza, F.F.; Fonseca, V.D.R.; Romão, W.; de Sairre, M.I.; Honorio, K.M.; Lacerda Jr, V.; Morais, P.A.B. Semisynthetic p-Coumaric Acid Derivatives as Lead Dual Inhibitors Against DPP-IV and GSK-3β for Antidiabetic Therapy. *Chem. Biol. Drug Des.* **2024**, *104*, e70016. [CrossRef]
48. Hua, L.; Anjum, F.; Shafie, A.; Ashour, A.A.; Almalki, A.A.; Alqarni, A.A.; Banjer, H.J.; Almaghrabi, S.A.; He, S.; Xu, N. Identifying promising GSK3β inhibitors for cancer management: A computational pipeline combining virtual screening and molecular dynamics simulations. *Front. Chem.* **2023**, *11*, 1200490. [CrossRef]

Disclaimer/Publisher's Note: The statements, opinions and data contained in all publications are solely those of the individual author(s) and contributor(s) and not of MDPI and/or the editor(s). MDPI and/or the editor(s) disclaim responsibility for any injury to people or property resulting from any ideas, methods, instructions or products referred to in the content.